Int. J. Electrochem. Sci., 11 **(2016)** 9542 – 9558, doi: 10.20964/2016.11.13

International Journal of
ELECTROCHEMICAL
SCIENCE
www.electrochemsci.org

Corrosion Behaviors of SMSS 13Cr and DSS 22Cr in H_2S/CO_2-Oil-Water Environment

Wei Yan[1], *Peike Zhu*[2], *Jingen Deng*[1]

[1] State Key Laboratory of Petroleum Resource and Prospecting, China University of Petroleum, Beijing102249, China
[2] PetroChina Research Institute of Petroleum Exploration & Development, Beijing, 100083, China
*E-mail: yanwei289@126.com

Received: 20 July 2016 / *Accepted:* 4 September 2016 / *Published:* 10 October 2016

A series of corrosion tests were performed in field and laboratory to investigate corrosion behaviors of Supermartensitic Stainless Steel 13Cr (SMSS 13Cr) and Duplex Stainless Steel 22Cr (DSS 22Cr) in H_2S/CO_2 containing environment. Carbon steel of P110S was chosen as comparison specimens in this study. A new field corrosion testing apparatus was designed and manufactured in order to perform this study. The corrosion species of the pipe flow include CO_2, H_2S and saline formation water; the water cut of the production flow was 16%. The flow temperature near the wellhead was 50°C, the corrosion test was 90 days. Analysis techniques, such as Weight loss, X-Ray Diffraction (XRD), Scanning Electron Microscope (SEM), Energy Dispersive Spectrum (EDS), double-loop electrochemical potentiokinetic reactivation (DL-EPR) and Scanning Kelvin Probe Force Microscopy (SKPFM) methods were used in this study. The results showed that pitting attack happened on DSS 22CR and P110S specimens, however, SMSS13Cr steel was survival. In high H_2S containing environment, the reactivation ratio of SMSS 13Cr was lower than DSS 22Cr and the intergranular corrosion and the degree of sensitization (DOS) of DSS 22Cr was higher, and the risk of localized corrosion in DSS 22Cr steel was higher. Corrosion mechanism models in H_2S/CO_2-oil-water system for the three types of steel were proposed.

Keywords: Corrosion; H_2S/CO_2-oil-water system; pitting attack; SMSS 13Cr; DSS 22Cr

1. INTRODUCTION

Exploration of the sour oilfields (containing H_2S or H_2S/CO_2) is becoming more common in recent decades years. Corrosion failure caused by H_2S or H_2S/CO_2 containing multiphase flow has affected the normal operation of the oil field, some production wells have to be shut down in a severe corrosion case. Kermani has reported that over 25% of failures in the oil and gas industry are related with corrosion. More than half of these failures are associated with produced oil and gas containing

H_2S and CO_2 [1]. In 1999, more than 1100 corrosion failures occurred in the oil and gas production system in Zhongyuan oilfield, among which 758 corrosion perforations occurred in wellhead pipeline [2]. Most of the corrosion failures are starting with corrosion pits, and then developing into a perforation and leakage. It is significant to conduct an investigation on pitting corrosion in the presence of H_2S and CO_2 environment of production pipeline or tubing [3-5]. In the presence of H_2S/CO_2 environment, iron sulfide is superior to precipitating on the steel surface compared with iron carbonate. The iron sulfide has an important role of preventing ion diffusion and protecting metal, however, the protective film property is determined by the concentration of H_2S [6-8]. Additionally, pH value has a great influent on the stability of ion sulfide.

Aqueous CO_2 corrosion of carbon and low alloy steels is an electrochemical process involving the anodic dissolution of iron and the cathodic evolution of hydrogen [9]. The electrochemical reactions are often accompanied by the formation of products such as $FeCO_3$ [10]. The overall reaction is:

$$Fe + CO_2 + H_2O \rightarrow FeCO_3 + H_2 \tag{1}$$

Iofa [11] presented that H_2S on the surface of iron formed ions and dipoles, their cathode point media. Thus, the reactions of iron in H_2S media include, in order, chemical adsorption reaction (Equation (2)) and anodic discharge reaction (Equation (3)):

$$Fe + H_2S + H_2O \rightarrow FeSH^-_{ads} + H_3O^+ \tag{2}$$

$$FeSH^-_{ads} \rightarrow FeSH^+_{ads} + 2e^- \tag{3}$$

Shoesmith [12] presented that $FeSH^+_{ads}$ may directly form FeS (Equation (4)) following the discharge reaction (Equation (5)) in a small amount of acid solutions but hydrolyze in mostly acid solutions:

$$FeSH^+_{ads} \rightarrow FeS + H^+ \tag{4}$$

$$FeSH^+_{ads} + H_3O^+ \rightarrow Fe^{2+} + H_2S + H_2O \tag{5}$$

The key factor of corrosion resistance alloys (CRA) for anti-corrosion is the passive films on the CRA surface, including the dissolution and self-repairing of the passive films. Once the passive films are locally damaged by the corrosive media, and can't effectively self-repair, local corrosion will occur. Sato [13] discovered the bipolar mechanism of the passive films. The outermost hydroxide layer prevents anions spreading to the inner layer of passive films and the innermost oxide layer prevents positive ions spreading to outer layer, thus the passive films protect the metal. The existence of CO_2 and H_2S may destroy the stability of passive films on high alloy steels and hamper the activation-passivation transition.

Super-martensitic stainless steel (SMSS) and duplex stainless steel (DSS) possess the outstanding corrosion resistance in CO_2 environment [14], due to the presence of the thin passive layer. Enrichment of chromium is a remarkable feature of the passive layer. Generally, the thickness of passive layer is only 1 to 3 nm, but it can decrease the corrosion rate significantly [15-17]. However, once the passivity film damaged in a localized zone, the big cathode area (passive film) will accelerate corrosion rate of the small anodic area (active point) and severely localized attack will occur [18]. SMSS has the advantages of low production and maintenance costs, good mechanical properties and corrosion resistance [19, 20]. DSS are characterized by a two-phase structure comprising a mixture of ferrite (α) and austenite grains (γ). The relationship (by volume) between both phases can vary between 30% and 70% but is usually about 50%. DSS also has the advantages of superior mechanical strength and corrosion resistance than common austenitic stainless steels, but with lower cost than nickel alloy. In general, chromium, molybdenum and nitrogen are beneficial alloying elements against pitting corrosion [21-22].

However, the study of corrosion behavior of stainless steels in the sour environment (H_2S or H_2S/CO_2) is relatively less and the corrosion mechanism is not fully understood. This paper presented the corrosion performance of SMSS 13Cr, DSS 22Cr and P110S by long-term tests in Missan oil field. These results will be significant to anti-corrosion material selection in high H_2S containing oil and gas field.

2. EXPERIMENTAL

2.1. Materials

The chemical compositions of SMSS 13Cr, DSS 22Cr and P110S are shown in Table 1. The optical microstructure of SMSS13Cr is uniform lath martensite and DSS 22Cr is both with ferrite and austenite phase, with ferrite (ɑ) appearing darker than austenite (γ), as shown in Figure 1 and Figure 2. The microstructure of P110S is tempered sorbite.

Table 1. Chemical compositions of SMSS13Cr, DSS 22Cr and P110S (wt.%).

Elements	C	Si	Mn	P	S	Cr	Ni	Cu	Mo	Fe
SMSS13Cr	0.029	0.20	0.38	0.02	0.001	12.78	5.12	0.06	2.23	balance
DSS 22Cr	0.023	0.62	1.29	0.025	0.0005	22.91	5.65	0.15	3.21	balance
P110S	0.25	0.21	0.51	0.0086	0.0024	1.06	0.025	_	0.65	balance

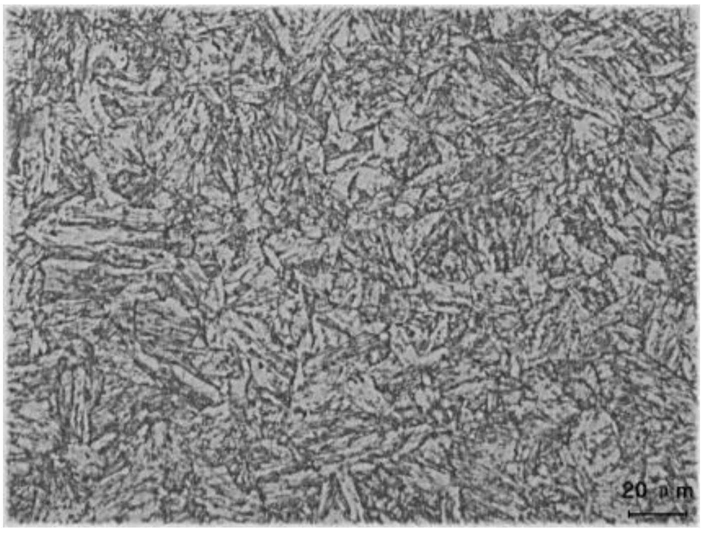

Figure 1. Optical microstructure of SMSS13Cr steel

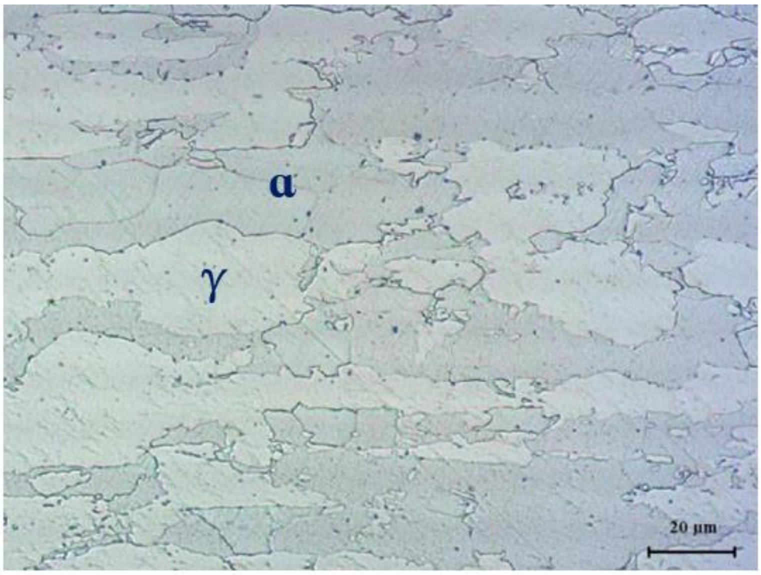

Figure 2. Optical microstructure of DSS 22Cr steel (α is ferrite phase; γ is austenite phase).

2.2. Production flow and water chemistry

Table 2 shows the parameters of production flow. High concentration of CO_2 and H_2S are containing in the production flow. The flow rate is 1.8m/s, and water cut is 16%. According to the previous study [23], the flow pattern inside the pipe is the dispersed flow. The pipe flow simulation by using the FLUENT software is shown in Figure 3; the simulation result is generally consistent with the previous study. The side wall specimens can be wetted by the production water (corrosion will happen).

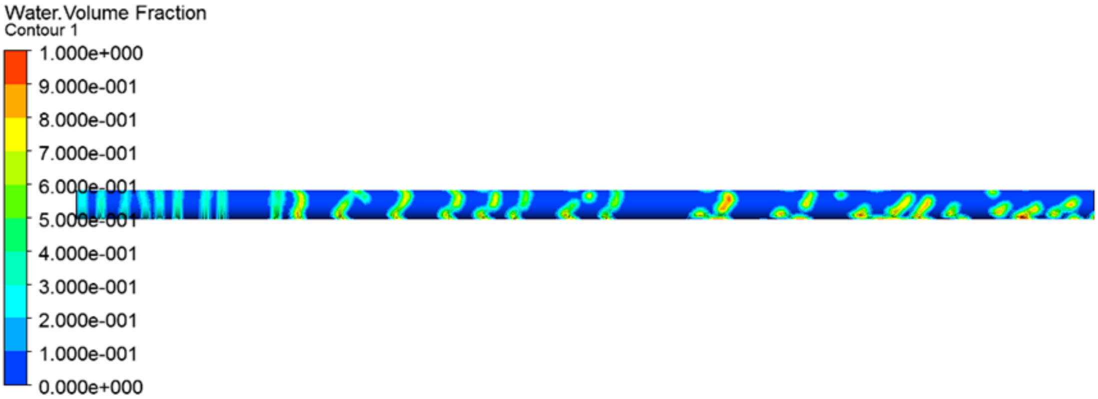

Figure 3. Simulation result of water volume fraction of the pipe flow. (calculation parameters: pipe line OD =152.4mm (6inch), wall thickness 5.56mm; two phase flow: phase 1 is oil, oil density 850kg/m^3, oil dynamic viscosity 0.02kg/m.s; phase 2 is water; water cut 16% ; inlet flow rate 1.8m/s)

Table 2. Operational conditions of the production pipeline, well#1, Missan oil field

Parameters	Values
CO_2 concentration, %	7.12
H_2S concentration, %	4.44
CO_2 partial pressure, MPa	0.13
H_2S partial pressure, MPa	0.08
Flow quantity (liquid), m3/day	91.58
Flow quantity (oil), m3/day	80.61
Flow quantity (water), m3/day	10.97
Water content, %	16
Flow rate, m/s	1.8
Temperature, ℃	50

The pH value of the formation water is 7.27 and the ion concentration of production water is shown in Table 3.

Table 3. water chemistry of production water (mg/L)

pH	Na^+	Ca^{2+}	Mg^{2+}	K^+	Cl^-	SO_4^{2-}	HCO_3^-
7.27	64870	14298	2137	1061	139552	951	417

2.3. Field corrosion testing method and specimen preparation

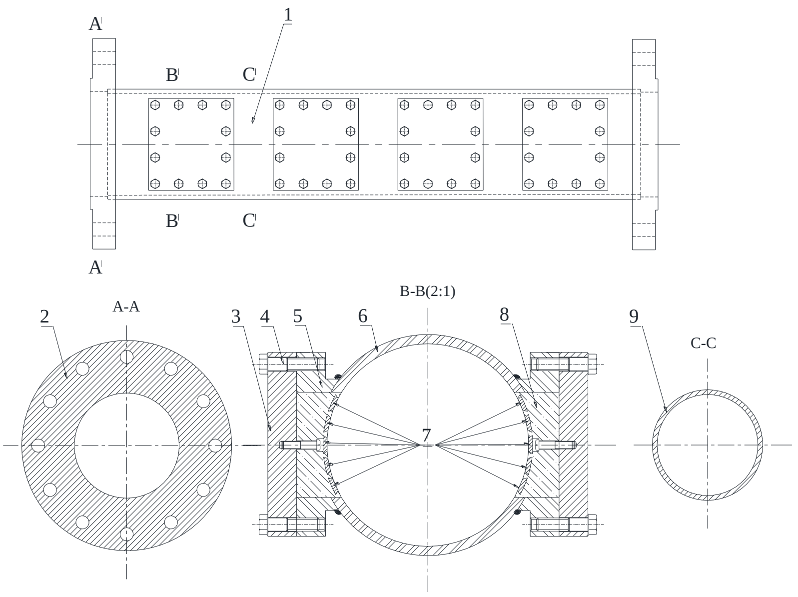

Figure 4. Oilfield test apparatus (1-field test apparatus; 2-flanged joint; 3-end shield; 4-stainless steel bolt; 5-pedestal; 6-body wall of field test apparatus at B-B; 7-specimens; 8-PTFE holder; 9-body wall of field test apparatus at C-C)

The test apparatus was specially designed for this study and connected directly to the production pipeline working as a production joint. The diagram of the cross section and main parts of test joint are shown in Figure 4 and Figure 5 respectively. The internal diameter of PTFE specimen holder is equal to the pipeline (Figure 5(a)). Thus, it was considered that the flow pattern does not change when production liquid passing through the test joint. In order to avoid the influence of solid deposit on corrosion behavior at the pipeline bottom, specimens were located at the both side walls of the test section (Figure 5(b)).

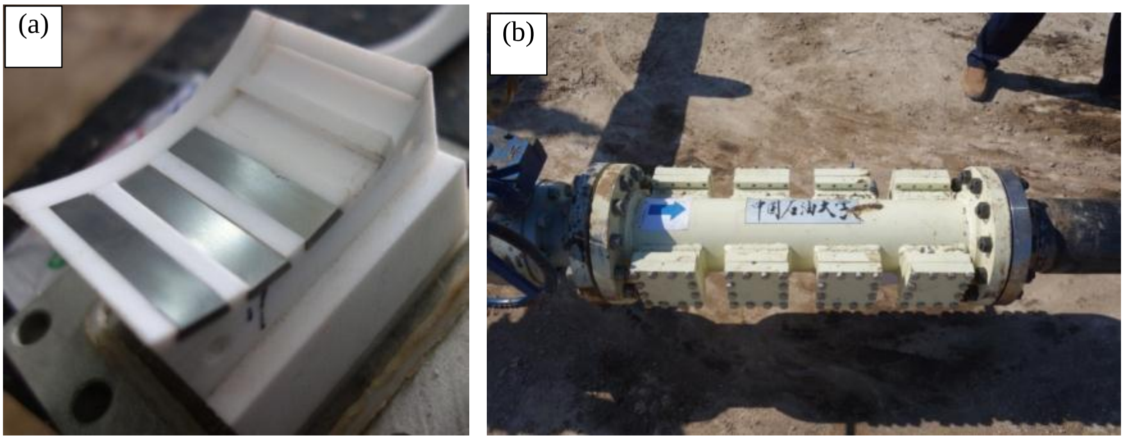

Figure 5. Field corrosion test joint. (a) Test specimens and PTFE coupon holder, (b) test joint after fixed in production pipeline.

The trapezoidal cross sectional shape specimens (T type specimens, 50mm × (12mm + 10mm) ×3mm) were used for field corrosion tests (Figure 5(a)). Prior to the field corrosion tests, specimens were polished with 320#, 600# and 800# sandpaper. Finally, all specimens were rinsed with acetone, washed with distilled water, dried with hot air and weighed using a four-decimal-digital balance. Specimens were divided into two groups, one is for weight loss determination and the other for surface morphology analysis. The corrosion test is 90 days.

2.4. Corrosion rate calculation

Corrosion rates were determined according to the NACE RP 0775-2005 standard [24]. The corrosion products were removed by using the chemical HCl (15%) with 5 mg/L of hexamethylenetetramine. These specimens were rinsed with distilled water, dried and weighed repeatedly until a stable mass loss values were obtained. Usually repeat 4-5 times.

The general corrosion rate and penetration rate were calculated using the following formulas:

$$\text{General corrosion rate (mm/a)} = \frac{365000 \times mass\ loss\ (g)}{Density\ (g{\cdot}cm^{-3}) \times Area(mm^{2}) \times exposure\ time\ (days)} \quad (6)$$

$$\text{Penetration rate (mm/a)} = \frac{\boldsymbol{depth\ of\ deepest\ pit\ (mm) \times 356}}{\boldsymbol{exposure\ time\ (days)}} \quad (7)$$

where, the density of 7.85g/cm^3 was used for the three types of steel.

2.5. Surface morphology analysis

Scanning electron microscopy (SEM, FEI Quanta 200F), Energy Dispersive Spectroscopy (EDS) and X-ray diffraction (D/MAX2500) were used to analyze the corrosion product. After corrosion products were removed, the surface of specimen was analyzed by SEM. Cross-section morphology was used to determine the profile and depth of pitting.

2.6. Double-loop electrochemical potentiokinetic reactivation

The DL-EPR (double-loop electrochemical potentiokinetic reactivation) test specimens include SMSS13Cr and DSS 22Cr. The test solution was 2 mol L^{-1} H_2SO_4 with 0.05 mol L^{-1} KSCN, at room temperature. The test conditions are including H_2S saturated and without H_2S. The tests were performed using a three-electrode cell system with a saturated calomel electrode (SCE) as a reference and a carbon rod as counter electrode and CS310 potentiostat.

The DL-EPR polarization curves were obtained after two steps: (1) the working electrode was subjected to open circuit conditions, until a steady state potential (E_{corr}) was reached; (2) An anodic potentiodynamic sweeping rate of 0.5 mV/s, from E_{corr} to +150 mV_{SCE}, was imposed. An anodic current peak, as I_a was measured. At +150 mV, the potential scanning was reversed to E_{corr} and the current peak during cathodic direction, as I_r was measured. The test results were expressed in the current densities's ratio, I_r/I_p*100.

2.7. Scanning kelvin probe force microscopy

Scanning Kelvin Probe Force Microscopy (SKPFM) method was used to measure the surface potential of DSS 22Cr steel. The surface morphology and contact potential difference around DSS 22Cr were obtained using a dimension atomic force microscope (AFM). The probes used in measurements were Pt-Ir-coated silicon tips. SKPFM is calibrated before testing with a standard specimen. Prior to the SKPFM measurements, 22Cr specimens were corroded in the certain solution (10mL HNO_3+30mL HCl+20mL CH_3CH_2OH) for 3-5 seconds. All measurements were conducted under the tapping mode by the mechanical excitation of cantilever and potential when a tip voltage is applied to the probe tip.

3. RESULTS AND DISCUSSION

3.1. Corrosion rates

Figure 6 shows the average corrosion rate of P110S, SMSS13Cr and DSS 22Cr in field production pipeline environment after 90 days test. Average corrosion rates of P110S, SMSS 13Cr and DSS 22Cr are 0.18mm/a, 0.10mm/a and 0.01mm/a respectively. Average corrosion rate of carbon steel is obviously higher than the other two stainless steels, and the corrosion rate of SMSS 13Cr is about ten times higher than DSS 22Cr.

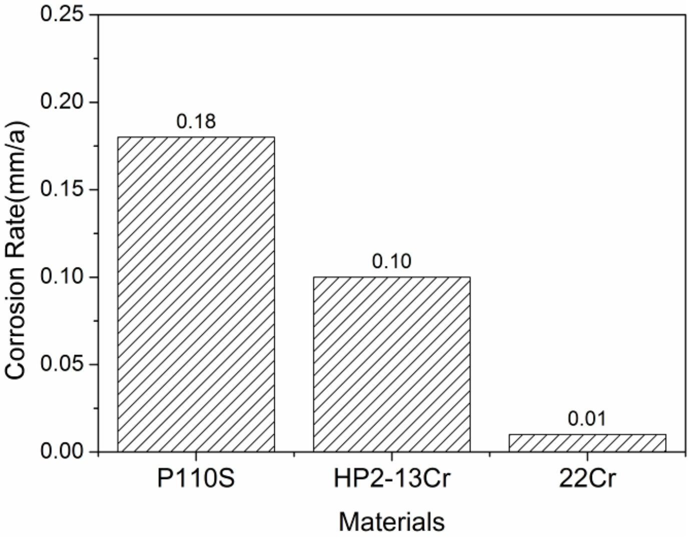

Figure 6. general corrosion rate of P110S, SMSS13Cr and DSS 22Cr steels (Temperature 50℃, CO_2 0.13MPa, H_2S 0.08MPa, flow rate 1.8m/s, water cut 16%, exposure 90 days)

3.2. Corrosion products

The corrosion product SEM micrograph of P110S steel is porous and there are many solids attached to the specimens' surface (Figure7a). EDS results shows that iron and sulfide are the dominated elements of the corrosion products, no chromium element peak appeared (Figure 7b). Combined with XRD results (Figure 8), a semi-stable form of FeS mackinawite was determined.

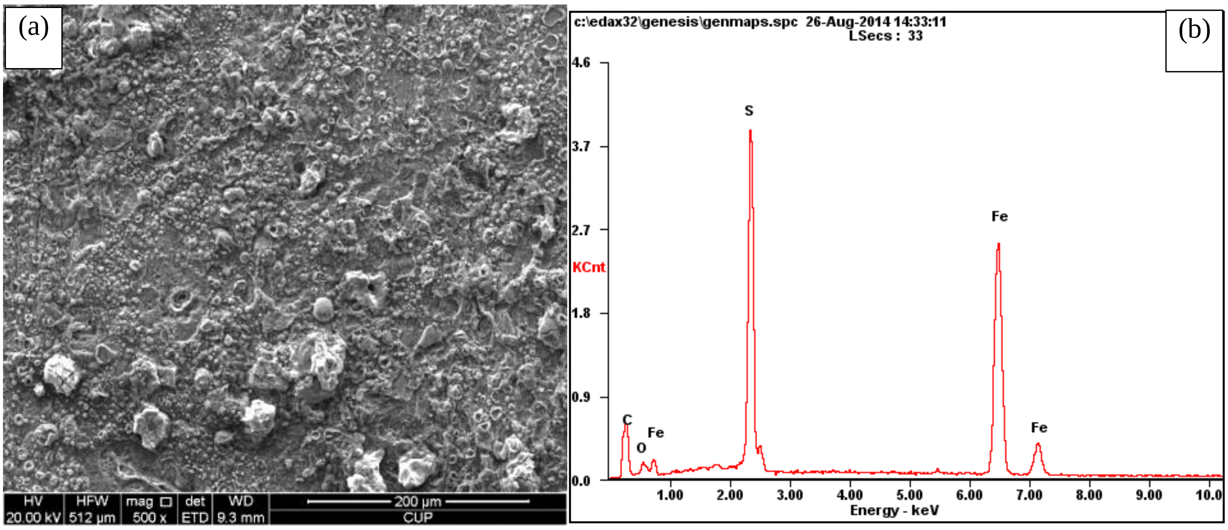

Figure 7. SEM picture and EDS map of P110S specimens. (a) SEM photo, ×500 times; (b) EDS map; (temperature 50℃, CO_2 0.13MPa, H_2S 0.08MPa, flow rate 1.8m/s, water cut 16%, exposure 90 days)

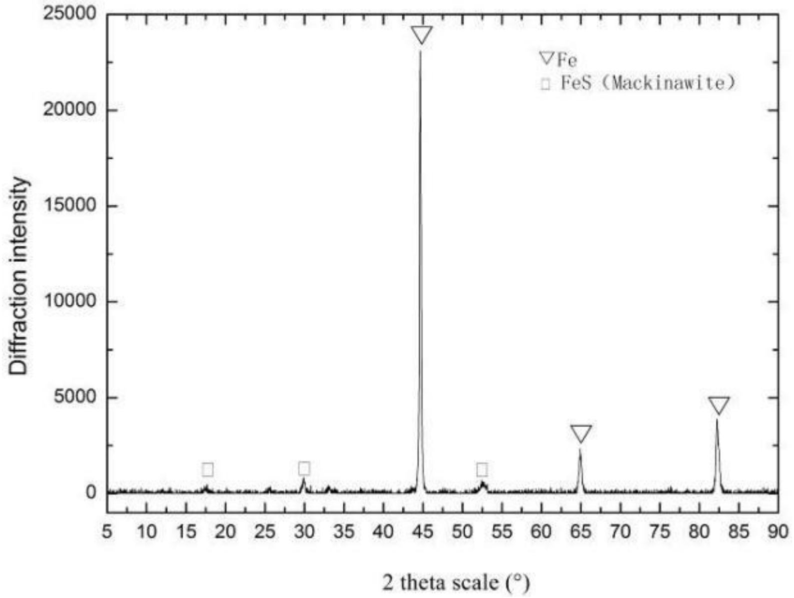

Figure 8. X-ray diffraction of corrosion product (temperature 50°C, CO_2 0.13MPa, H_2S 0.08MPa, flow rate 1.8m/s, water cut 16%, exposure 90 days)

Compared to the P110S, SMSS 13Cr performed well under the same conditions. Almost no corrosion scales formed on the samples' surface (Figure 9a). No localized corrosion was observed in the SEM photos. A high content (about 15%wt) of chromium appeared in the EDS map (Figure 9b).

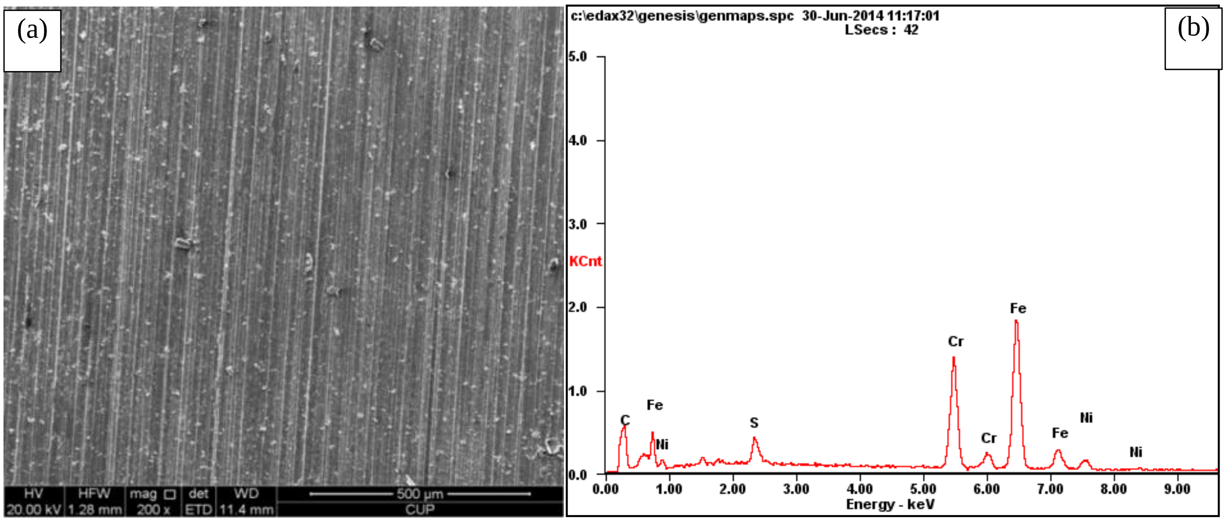

Figure 9. SEM picture and EDS map of SMSS13Cr specimens (a) SEM picture, ×200 times; (b) EDS map (temperature 50°C, CO_2 0.13MPa, H_2S 0.08MPa, flow rate 1.8m/s, water cut 16%, exposure 90 days)

However, the corrosion performance of DSS 22Cr steel was quite unexpected. Although the general corrosion rate is the lowest, some corrosion pits appeared on the sample surface (Figure 10a). EDS analysis shows that chromium and iron are the main elements in the products, and sulfur, nickel, molybdenum, silicon, calcium, chlorine and are also detected (Figure 10b). In a purely CO_2 corrosion environment, the corrosion resistance is usually correlated the chromium content, a higher chromium content implies a better resist ability to corrosion (both general corrosion and localized corrosion). Thus, 22% wt of Cr content steel (DSS 22Cr) should perform better than 13%wt Cr content steel (SMSS 13Cr). Nevertheless, the presence of high concentration of H_2S changed this traditional understanding totally [25].

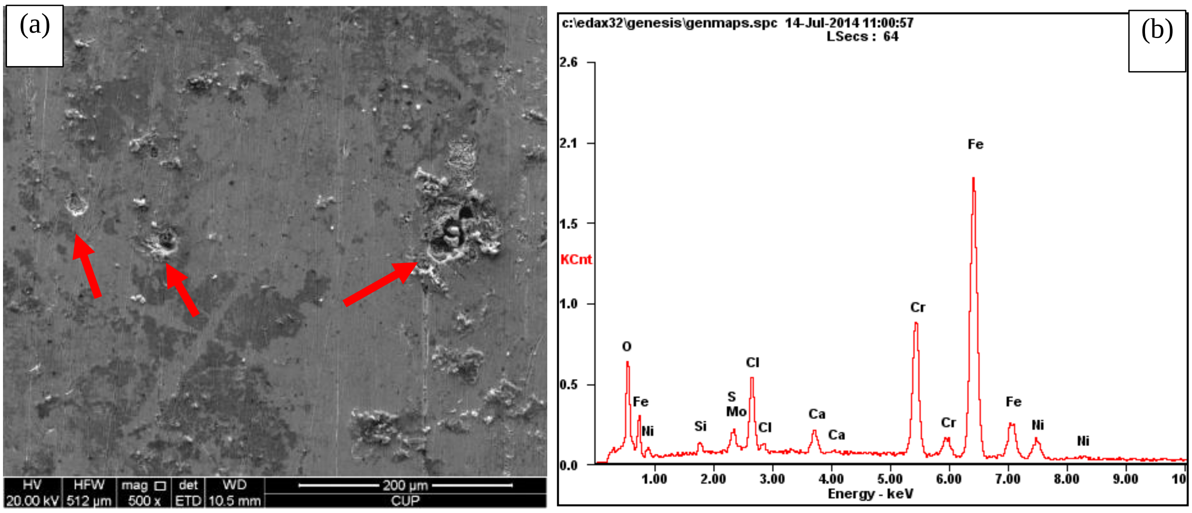

Figure 10. SEM picture and EDS map of DSS 22Cr specimens (a) SEM picture, ×500 times; (b) EDS map (temperature 50℃, CO_2 0.13MPa, H_2S 0.08MPa, flow rate 1.8m/s, water cut 16%, exposure 90 days)

3.3. Surface morphologies after removing the scales

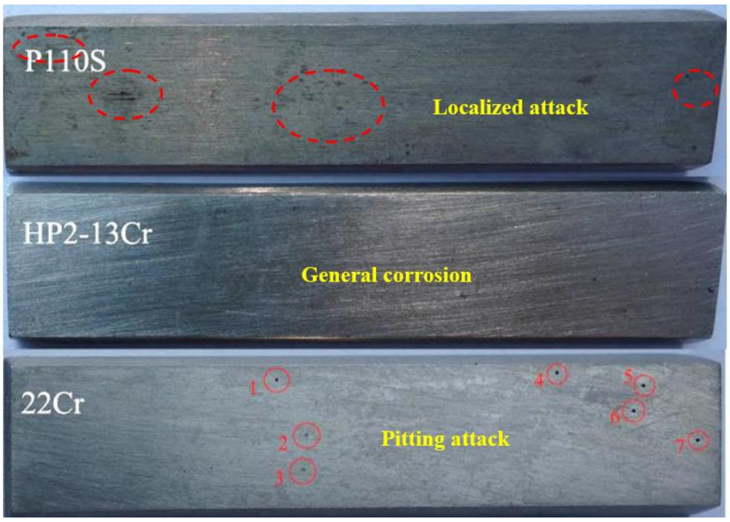

Figure 11. photographs of P110S, SS13Cr and 22Cr specimens after removing corrosion scale (temperature 50°C, CO_2 0.13MPa, H_2S 0.08MPa, flow rate 1.8m/s, water cut 16%, exposure 90 days)

After a corrosion product was removed, SEM pictures of P110S, SMSS13Cr and DSS 22Cr are shown in Figure 11. It can be observed by naked eyes that several localized corrosion zones appeared in the P110S specimen surface (red dash line circles). All of SMSS13Cr specimens were survival from localized corrosion, only general corrosion was observed. Most of the DSS 22Cr specimens occurred pitting corrosion. As shown in the picture, several pits were observed in the specimen by naked eyes (red line circles).

The SEM pictures (Figure 12) of the three types' specimens are matched with the photographs in Figure 11, pitting corrosion was observed both in P110S and DSS 22Cr specimens (Figure 12 a and c), but the SMSS13Cr steel was survival (Figure 12b).

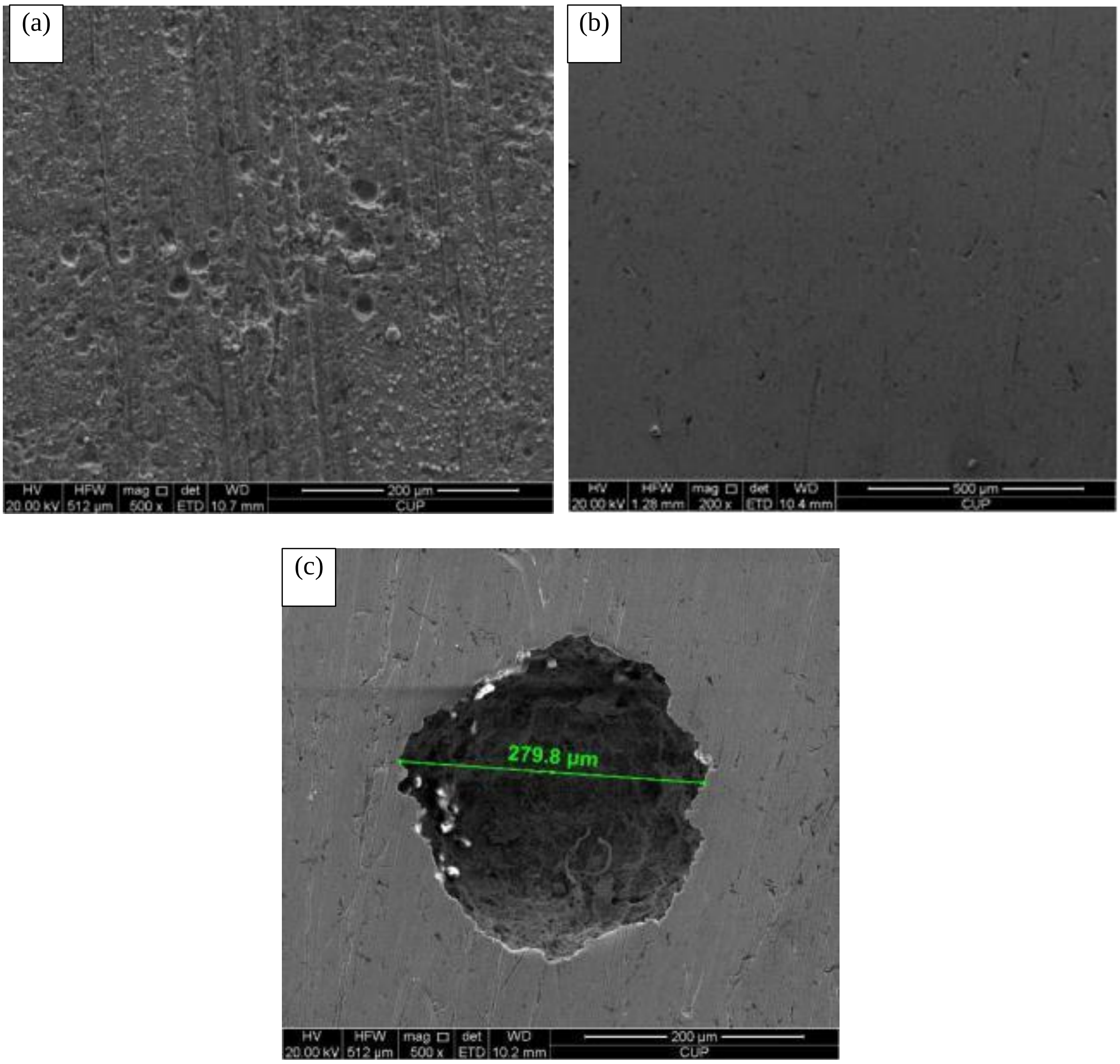

Figure 12. SEM pictures after removing the scale (a) P110S, ×500 times; (b) SS13Cr, ×200 times; (c) DSS 22Cr, ×500 times. (temperature 50℃, CO_2 0.13MPa, H_2S 0.08MPa, flow rate 1.8m/s, water cut 16%, exposure 90 days)

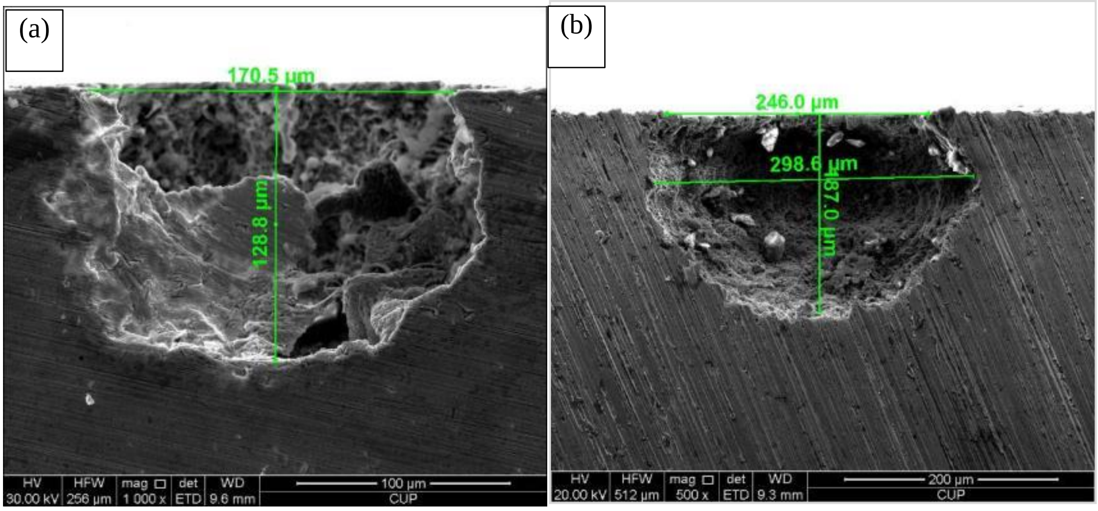

Figure 13. SEM pictures of cross sections (a) P110S, ×1000 times; (b) DSS 22Cr ×500 times. (Temperature 50℃, CO_2 0.13MPa, H_2S 0.08MPa, flow rate 1.8m/s, water cut 16%, exposure 90 days, penetration rate of P110S 0.52 mm/a, penetration rate of DSS 22Cr 0.76mm/a)

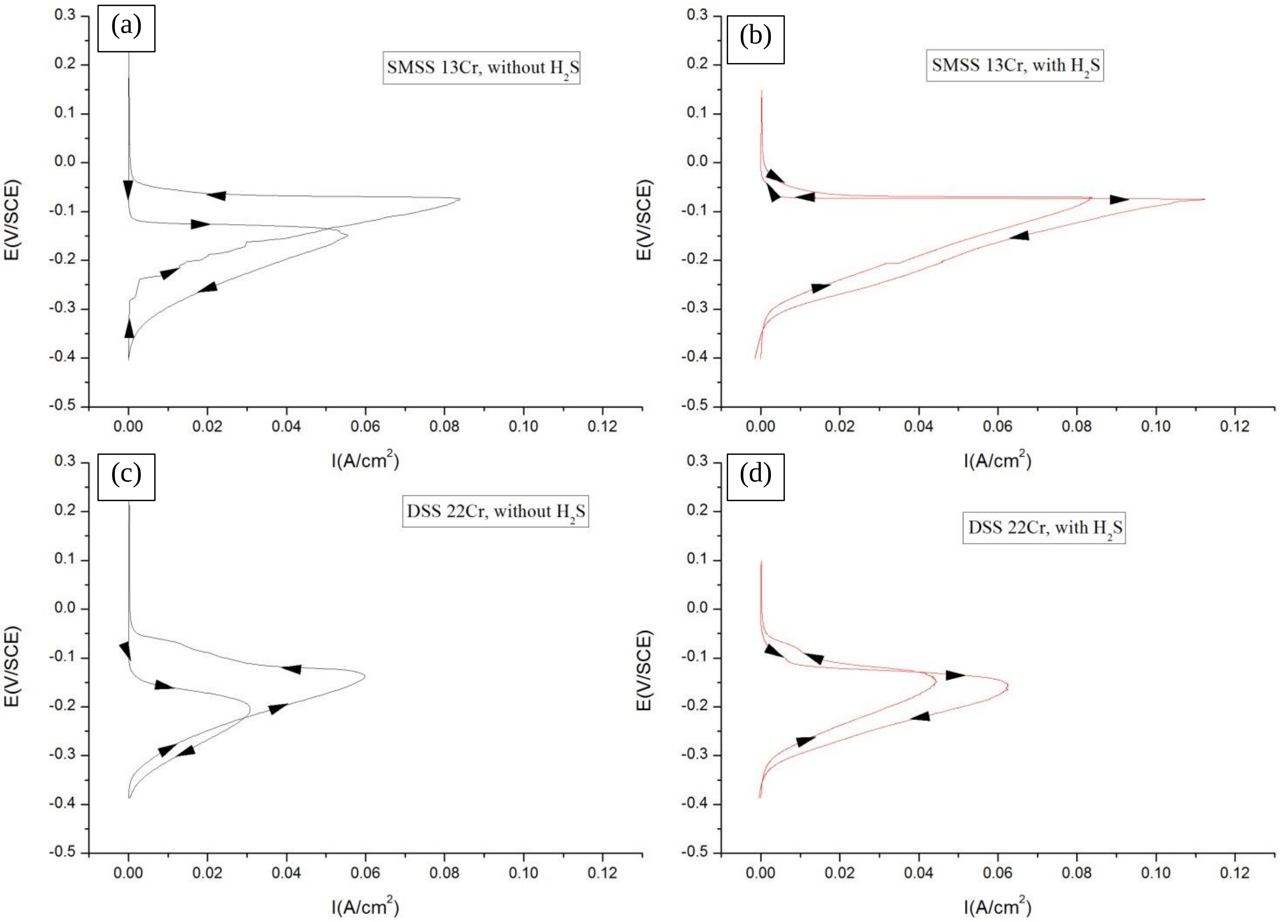

Figure 14. DL-EPR curves of SMSS 13Cr and DSS 22Cr under different conditions (a) SMSS 13Cr, no H_2S; (b) SMSS 13Cr, with H_2S; (c) DSS 22Cr, no H_2S; (d) DSS 22Cr, with H_2S. (Test solution 2 mol L^{-1} H_2SO_4 with 0.05 mol L^{-1} KSCN, room temperature, sweeping rate 0.5 mV/s, from E_{corr} to +150 mV_{SCE})

As the SEM cross-sectional pictures shown in Figure 13, the pit depth of P110S specimen is 128.8μm, get a penetration rate of 0.52mm/a according to the formula (2); the pit depth of DSS 22Cr is 187.0μm, get a penetration rate of 0.76mm/a. The pits show a typical shape characteristic of pitting corrosion, which is usually called “sack shape” (small opening with a big belly). The penetration rate of DSS 22Cr is even higher than the carbon steel.

3.4. DL-EPR test results

Figure 14 shows the DL-EPR test results. In the condition of no H_2S, reactivation ratio of MSS 13Cr is higher than DSS 22Cr, however, after H_2S saturated, the current density of SMSS 13Cr and DSS 22Cr are both dramatically increased, but the reactivation ratio of SMSS 13Cr is lower than DSS 22Cr. In H_2S-saturated solution, intergranular corrosion and DOS (degree of sensitization) of 22Cr is higher than SMSS 13Cr, localized corrosion resistance of DSS 22Cr is dramatically decreased (Figure 15). This result can support the field test results that the DSS 22Cr is more easily to be attacked by pitting corrosion compared to the SMSS 13Cr in high H_2S presence environment.

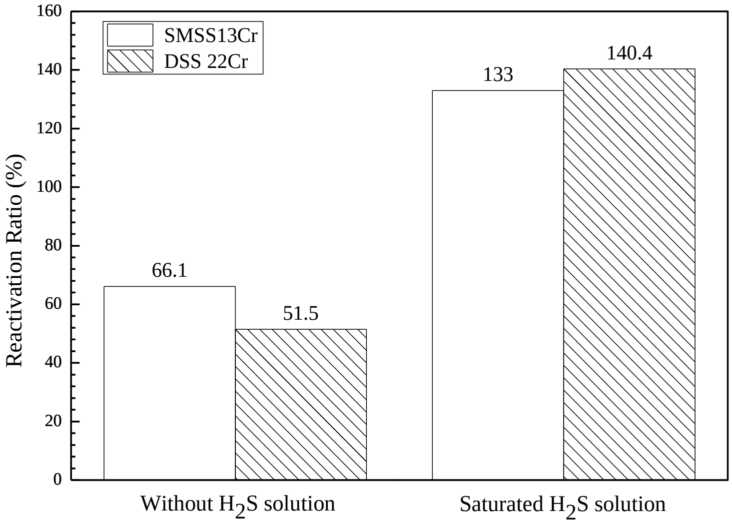

Figure 15. Reactivation ratio of SMSS13Cr and DSS 22Cr under different conditions (Test solution 2 mol L^{-1} H_2SO_4 with 0.05 mol L^{-1} KSCN, room temperature, sweeping rate 0.5 mV/s, from E_{corr} to +150 mV_{SCE})

3.5. SKPFM measurements results

The SKPFM mapping of morphology and Volta potential was performed on the polished and corroded specimen surface of DSS 22Cr to evaluate the relative corrosion tendency. The concurrent AFM morphology and Volta potential images of 22Cr are shown in Figure 16. The higher (brighter, green dash line circled) surface of the area is austenite phase, as the right marker in Figure 16a and Figure 16b, its height is about 20.71nm and Volta potential is about 10.19mV. The darker surface of the area was ferrite phase (yellow dash line circled), as the left marked point in Figure 16b, its height is about -19.27nm and Volta potential is about -22.87mV. The height and Volta potential of austenite point are all higher than ferrite point. The potential difference between austenite phase and ferrite phase is 33.06mV.

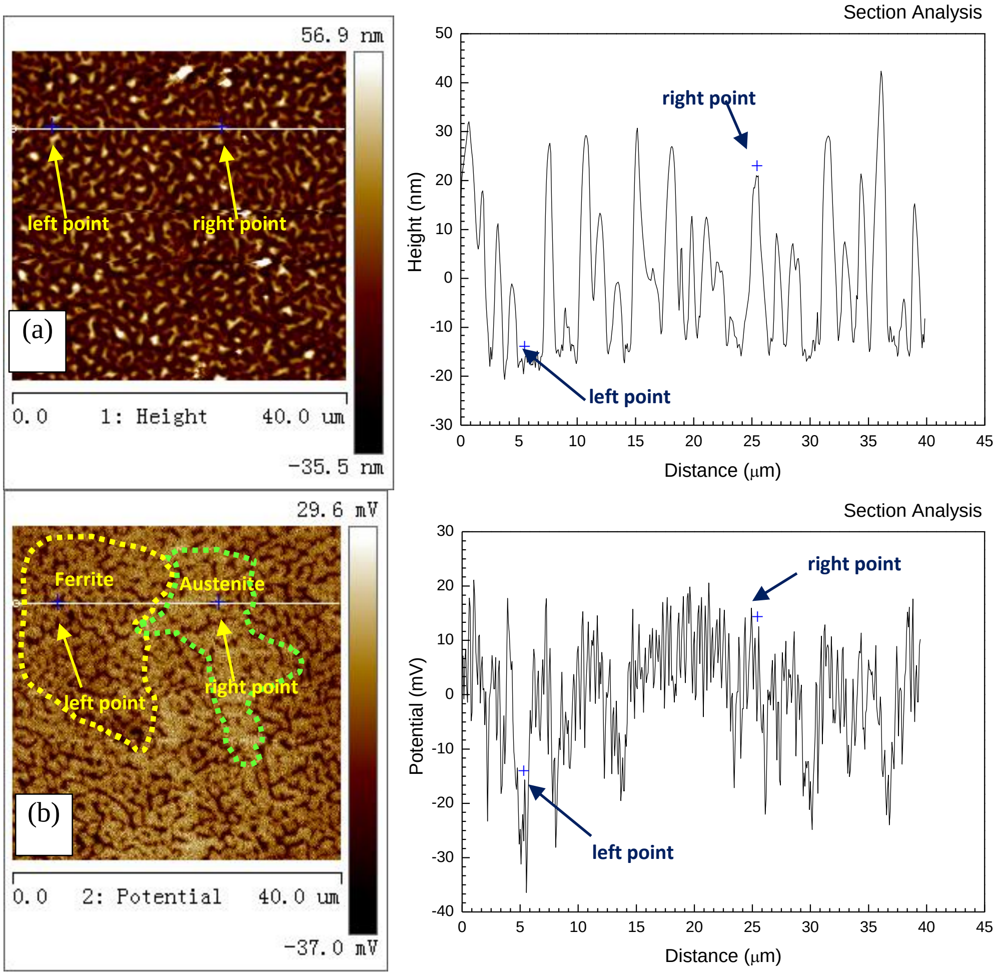

Figure 16. Topography and surface potential (SKPFM) images of 22Cr specimen, (a) section analysis of morphology; (b) section analysis of surface potential (Before the SKPFM measurements, the specimens were corroded in the solution "10mL HNO_3+30mL HCl+20mL CH_3CH_2OH" for 3-5 seconds)

3.6. Corrosion mechanism models in H_2S/CO_2-oil-water system

In CO_2/H_2S environment, carbon steel (e.g. P110S) can't form a passive layer because of the lack of chromium and nickel elements, the main corrosion products of carbon steel are iron carbonate and multiple forms of iron sulfide [6, 8, 14]. Passive layer can form on the stainless steel surface, such as SMSS13Cr and DSS 22Cr steels. The chromium enrichment passive layer can prevent the aggressive ions transferring and protect metal from corroding by the corrosive media [15-17]. With the increase of chromium content in alloy, the corrosion resistance getting enhanced, this is the main reason for the average corrosion rate of DSS 22Cr is lower than SMSS13Cr.

However, the corrosion resistance of ferrite phase in DSS 22Cr is inferior to austenite phase, hence the ferrite phase is easy to dissolve because of the galvanic cell [26]. The intergranular corrosion occurred generally in areas surrounding the austenite phases [27]. Additionally, the solid particles from the reservoir could damage the passive layer, and then chloride ions accumulate inside the weak point to start pitting corrosion. Large cathode area (passivate area) will accelerate corrosion of small anodic area (active point). Metal ions which dissolve at the anode, such as Fe^{2+}, Cr^{3+} and Ni^{2+} react with water to form H^+. Then, the pH value of media inside the pit is decreased and the metal's dissolution is accelerated. In order to keep the electric neutrality of media, lots of Cl^- move into the pit and bind metal ions. High concentration of chloride ions in formation water increase the activity coefficient of H^+ and prevent the reactivation of anodic area in pit. The autocatalytic effect of localized corrosion makes the pitting rate is considerably larger than the uniform corrosion rate [28]. The microstructure of SMSS 13Cr is single martensitic phase, and no selective dissolution of metal substrate occurred. Passive layer of SMSS 13Cr seems more stable than DSS 22Cr in Missan field condition.

According to the Al-Yaari's study [23], the continuous phase is oil, the dispersed phase is aqueous and the stable water-in-oil emulsion is formed. The adsorbed crude oil on the metal surface may diminish the contact between aqueous phase and metal. The inhibitive organic components which adsorbed onto the metal surface serve as a physical barrier to suppress the anodic reaction and cathodic reaction in corrosion process and diminish the corrosion of metal caused by aqueous phase. However, the physical barrier effect is not stable because of the flush of the multiphase flow. The dispersed aqueous phase may contact with metal intermittently to cause corrosion.

Based on the test results in this study, the author suggests that the corrosion behaviors of SMSS 13Cr and DSS 22Cr are significantly impacted by crude oil. The schematic of corrosion film of the three type of metal in H_2S/CO_2- oil-water multiphase flow is shown in Figure 17. The inhibitive organic components in crude oil adsorbs onto the metal surface non uniformly. The dispersed aqueous phase may touch the metal under the influence of high velocity flow. CO_2, H_2S and Cl^- dissolved in the water droplets to work as corrosion species. In addition, FeS, as the main corrosion products, formed very fast on to the steel surface [29]. The corrosive ions may locally penetrate the corrosion scales and cause pitting corrosion of metal.

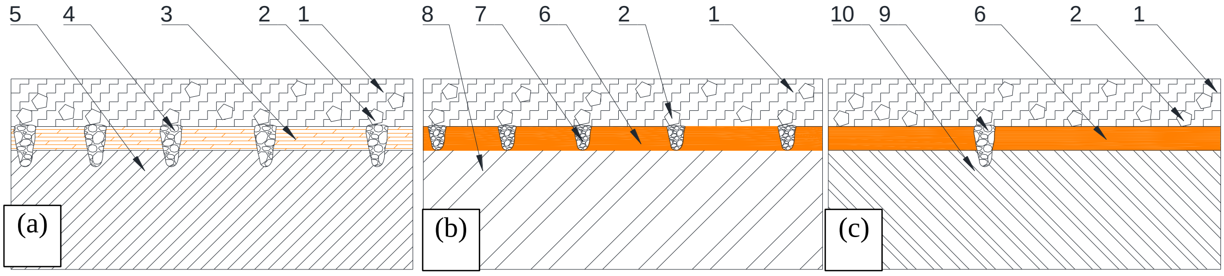

Figure 17. The schematic of corrosion film of the three type of metal in H_2S/CO_2- oil-water multiphase flow, (a)P110S, (b)SMSS 13Cr and (c) DSS 22Cr,1-crude oil ; 2-water ; 3-corrosion scales ; 4-pitting ; 5-matrix of P110S ; 6-passive films ; 7-local breakdown of passive films on SMSS ; 8-Matrix of SMSS SS13Cr ; 9-local breakdown of passive films on DSS ; 10-Matrix of DSS 22Cr

The microstructure of SMSS 13Cr is single phase martensite. Passive films can form on SMSS 13Cr in the CO_2/H_2S-oil-water environment. When the high speed dispersed flow pass through the pipeline, the passive films may be locally destroyed. However, the protective effect for substrate of passive film on SMSS 13Cr is inferior to DSS 22Cr, thus, the local breakdown of its passive films may easily transform into general corrosion (Figure 17b). Meanwhile, due to the pure phase microstructure, the passive film of SMSS 13Cr is more easily to be self-repaired.

Due to the different electrochemical potential of ferrite phase and austenite phase in DSS 22Cr, micro corrosion galvanic cell may form and induce the localized corrosion. Austenite phase of DSS 22Cr has a more positive potential acting as the anode to diminish the passive film self-repairing. In the presence of H_2S environment, the intergranular corrosion susceptibility is significantly increased. Big cathode area (passivate films) will accelerate corrosion of small anodic area (active point) and pitting progress. In addition, the acidification of media inside the pits and the enrichment of Cl^-, S^{2-} and HS^- may also diminish the self-repairing of passive films, accelerate dissolving metal and exacerbate pitting corrosion further (Figure17c).

4. CONCLUSIONS

The corrosion behaviors of SMSS 13Cr and DSS 22Cr in H_2S/CO_2-oil-water multiphase flow were investigated through the long term field test and a series of laboratory analysis. The flowing conclusions were obtained:

(1) The average corrosion rate of DSS 22Cr was the lower than SMSS 13Cr, but several pitting attack occurred. The penetration rate was 0.76 mm/a and the pit shows a typical shape of “small opening with a big belly”. This type of pit tends to have higher penetration rate than an open hole pit.

(2) All of SS13Cr specimens only occurred uniform corrosion. The general corrosion rate of SMSS13Cr is 0.10 mm/a.

(3) In the no H_2S condition, reactivation ratio of SMSS 13Cr was higher than DSS 22Cr, however, this result was changed after H_2S added, and the reactivation ratio of DSS 22Cr became higher. In H_2S-saturated solution, intergranular corrosion and DOS (degree of sensitization) of 22Cr was higher than SMSS 13Cr. DSS 22Cr has a higher risk of localized attack.

(4) The potential difference between austenite phase and ferrite phase is over 30 mV. It will have a significant effect on intergranular corrosion and be disadvantageous to the passive layer self-repairing.

(5) According to the laboratory analysis, mechanism models of the three type of metal in H_2S/CO_2- oil-water multiphase flow were proposed. SMSS13Cr shows a superior pitting resistance compared to DSS 22Cr, moreover, it has a lower cost than DSS 22Cr. Thus, SMSS 13Cr is recommended in this oil field.

ACKNOWLEDGEMENTS
The authors would like to thanks the sponsor company of China National Offshore Oil Corporation (CNOOC) , Iraq limited for their full support.

References

1. M.B. Kermani and D.Harrop, *SPE Production & Facilities.* 11(1996) 186-190
2. M. X. Lu, Z. Q. Bai, X.W. Zhao,J.H. Luo, C.F. Chen, *Corrosion & Protection.* 23(2002)105-113
3. S. D. Kapusta, B. F. M. Pots, R. A. Connell, *Corrosion, NACE International,* (1999) paper No.45.
4. G. Svenningsen, P. Attila, K. Jon, *Corrosion, NACE International,* (2009) paper No.09359.
5. A. Miyasaka, D. Kozo, O. Hiroyuki, *SPE production engineering*. (1998), paper No. SPE15804.
6. Z.F. Yin, W.Z. Zhao, Z.Q. Bai, *Electrochimica Acta*. 53(2008)3690-3700.
7. B. Kermani, J. W. Martin, K. A. Esaklul, *Corrosion, NACE International,*(2006) paper No. 06121
8. W. Yan, J. G. Deng, P. K. Zhu, X. J. Xing, *Corrosion Engineering, Science and Technology*. 50(2015)525-532
9. Y.H. Lin, A. Singh, E. E. Ebenso, M. A. Quraishi, Y. Zhou, Y. Huang, *Int. J. Electrochem. Sci.* 10 (2015) 194- 208.
10. S. Nesic, *Corrosion Science*, 49 (2007) 4308- 4338.
11. Z.A. Iofa, V.V. Batrakov , Cho-Ngok-Ba, *Electrochimica Acta*,12 (1964): 1645 –1653.
12. D. W. Shoesmith, P. Taylor, M. G. Bailey, D. G. Owen, *Journal of Electrochemical Society*,127 (1980) 1007-1015.
13. N. Sato, *Corrosion*, 45(1989)354-368.
14. L.J. Mu and W.Z. Zhao, Corrosion science. 52(2010)82-89.
15. H. Fischmeister and U. Roll, *Fresenius Journal of Analytical Chemistry*. 319(1984)639-645
16. C.-O.A. Olsson and D. Landolt, *Electrochimica Acta* , 48(2003) 1093-1104.
17. D. Sidorin, D. Pletcher, B. Hedges, Electrochimica Acta, 50(2005) 4109- 4116.
18. M. Ueda, K. Nakamura, N. Hudson, *Corrosion, NACE International*, (2003) paper No.03097
19. M. Herve, E. A. Hafida, L. Jean. *Corrosion, NACE International*, (2009) paper No.09084
20. D. K. Russell and S. C. Michael, *Corrosion, NACE International*,(1998) paper No.274
21. J. Shu, H. Bi, X. Li, Z. Xu, *Corrosion Science*, 57 (2012) 89-98.
22. R. Merello, F.J. Botana , J. Botella, M. V. Matres, M. Marcos, *Corrosion Science,*45(2003) 909-921.
23. M. A. Al-Yaari and B. F. Abu-Sharkh, *Asian Transactions on Engineering,*1 (2011) 68-75
24. National Association of Corrosion Engineers, NACE (2005) RP 0775
25. X. L. Cheng, H. Y. Ma , S. H. Chen, L. Niu, S. B. Lei, R. Yu, Z. M. Yao,
26. L. F. Garfias-Mesias, J. M. Sykes, C. D. S. Truck, *Corrosion science,*38(1996)1319-1330.
27. B.H.Lee, H.W.Lee, Y. T. Shin. *Int. J. Electrochem. Sci*., 10 (2015) 7535 – 7547.
28. *Corrosion Science,* 41(1999) 773-788.
29. H. Shuji, M. Katsumi, Y. Kazuo, *Corrosion, NACE International*,(2003) paper No.03095
30. Y.G. Zheng, B. Brown, S. Nesic, *Corrosion*, 70(2014) 351-365